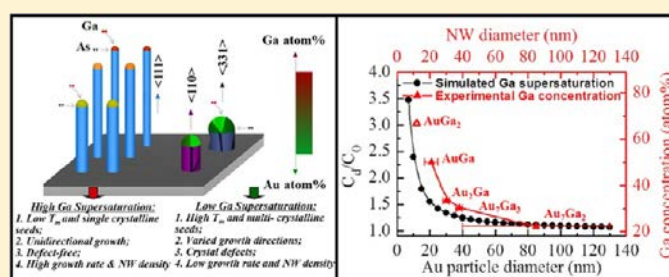# Manipulated Growth of GaAs Nanowires: Controllable Crystal Quality and Growth Orientations via a Supersaturation-Controlled Engineering Process

Ning Han,[†,⊥] Fengyun Wang,[†,⊥] Jared J. Hou,[†] SenPo Yip,[†] Hao Lin,[†] Ming Fang,[†] Fei Xiu,[†] Xiaoling Shi,[†] TakFu Hung,[†] and Johnny C. Ho*,[†,‡]

[†]Department of Physics and Materials Science, and [‡]Centre for Functional Photonics (CFP), City University of Hong Kong, Tat Chee Avenue, Kowloon, Hong Kong S.A.R., P. R. China

S *Supporting Information*

ABSTRACT: Controlling the crystal quality and growth orientation of high performance III–V compound semiconductor nanowires (NWs) in a large-scale synthesis is still challenging, which could restrict the implementation of nanowires for practical applications. Here we present a facile approach to control the crystal structure, defects, orientation, growth rate and density of GaAs NWs via a supersaturation-controlled engineering process by tailoring the chemical composition and dimension of starting Au_xGa_y catalysts. For the high Ga supersaturation (catalyst diameter < 40 nm), NWs can be manipulated to grow unidirectionally along ⟨111⟩ with the pure zinc blende phase with a high growth rate, density and minimal amount of defect concentration utilizing the low-melting-point catalytic alloys ($AuGa$, Au_2Ga, and Au_7Ga_3 with Ga atomic concentration > 30%), whereas for the low Ga supersaturation (catalyst diameter > 40 nm), NWs are grown inevitably with a mixed crystal orientation and high concentration of defects from high-melting-point alloys (Au_7Ga_2 with Ga atomic concentration < 30%). In addition to the complicated control of processing parameters, the ability to tune the composition of catalytic alloys by tailoring the starting Au film thickness demonstrates a versatile approach to control the crystal quality and orientation for the uniform NW growth.

II–V compound semiconductor nanowires (NWs) such as gallium arsenide (GaAs) and indium arsenide (InAs) are promising active materials for next-generation electronics, photonics and optoelectronics due to their remarkably high carrier mobility, direct and suitable bandgap for efficient photon coupling.[1–3] These NW materials are typically prepared adopting catalytic vapor–liquid–solid (VLS) and/or vapor–solid–solid (VSS) mechanisms on crystalline substrates in metalorganic chemical vapor deposition (MOCVD) or molecular beam epitaxy (MBE).[4–6] Despite the recent advances in NW synthesis, the as-grown NWs usually have a mixed crystal phase of zinc blende (ZB) and wurtzite (WZ), and twin planes or stacking defaults along the growth direction of NW, attributed to the small amount of formation energy difference between WZ and ZB structures in the nanoscale.[5,7–9] All these mixed crystal phase and growth orientations would greatly restrict the implementation of NWs for practical technologies. In particular, the mixed phase InAs NWs have an electrical resistivity up to 2 orders of magnitude higher than that of single phase NWs,[8] and the electronic bandgap of WZ GaAs NWs is 29 meV higher than that of ZB GaAs NWs,[10] which results in a

blue-shift of the corresponding light absorption and emission. For large-scale and device applications, it is highly desirable to prepare pure phase, unidirectional, and defect-free NWs with uniform performances.

Recently, Dick et al.[7] and Joyce et al.[11] have reported the growth control of pure ZB and WZ III–V NW phase by tuning basic process parameters, such as V/III ratio and growth temperatures in the Au-catalyzed MOCVD system: high V/III ratio and low temperature favor pure ZB NWs, while low V/III ratio and high temperature are suitable for pure WZ NW growth; however, it is also found that a too high V/III ratio would kink the NWs and increase the tapering, sacrificing the crystallinity and morphology for the phase control.[12] Nowadays, as noncrystalline substrates such as glass[13] and SiO_2[14] are more favored as to reduce the NW preparation cost and to enable heterogeneous integration of NWs such as via contact printing,[15,16] extensive efforts have been made to manipulate
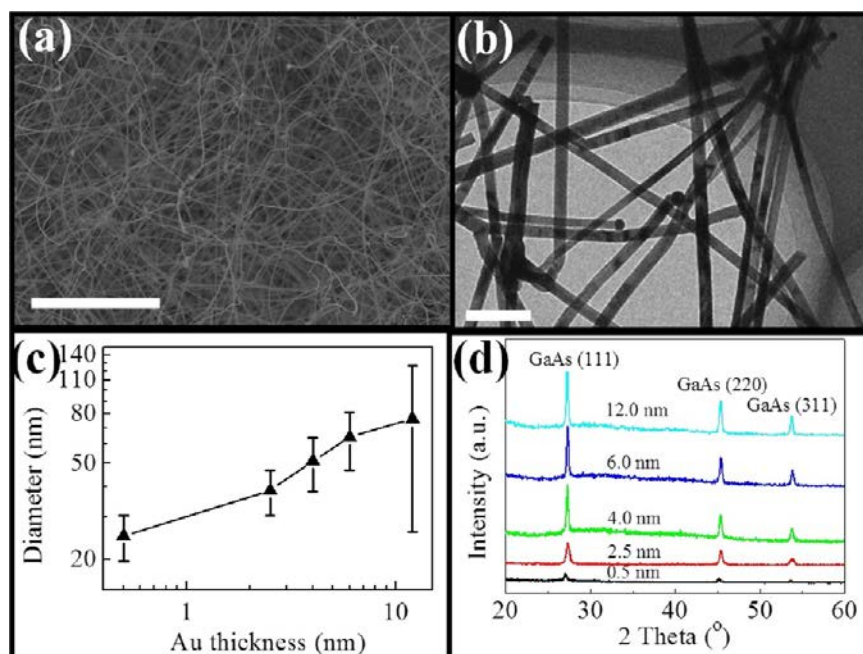
Figure 1. (a) SEM image of GaAs NWs prepared by the 4.0 nm thick Au catalyst film, (b) corresponding TEM image for the diameter distribution statistic, (c) diameter statistics of GaAs NWs prepared by 0.5 nm, 2.5 nm, 4.0 nm, 6.0 and 12.0 nm thick Au films, respectively, and (d) XRD patterns of GaAs NWs prepared by different thickness of Au catalyst films.
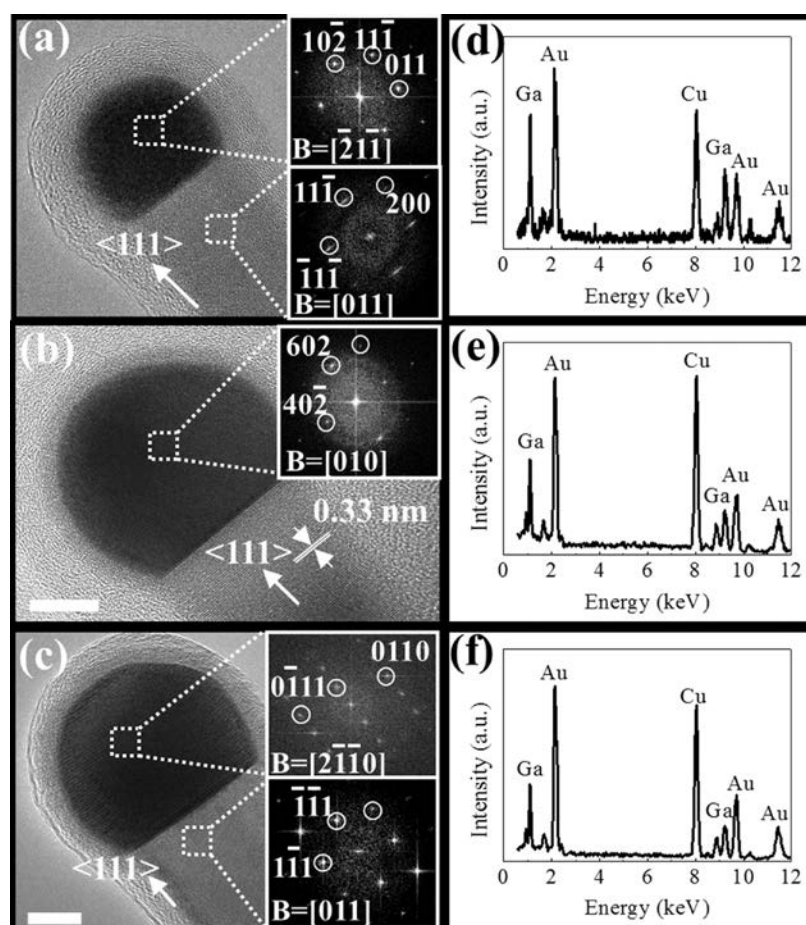

Figure 2. HRTEM images and corresponding FFT of thin NW tips and bodies (insets) grown by single crystalline Au−Ga alloy catalysts: (a) NW grown by AuGa catalyst (d = 25 nm), (b) NW grown by Au_2Ga catalyst (d = 27 nm), and (c) NW grown by Au_7Ga_3 catalyst (d = 38 nm). Scale bars = 10 nm. And (d−f) are the corresponding EDS spectra of the Au_xGa_y catalyst seeds of (a−c), respectively.
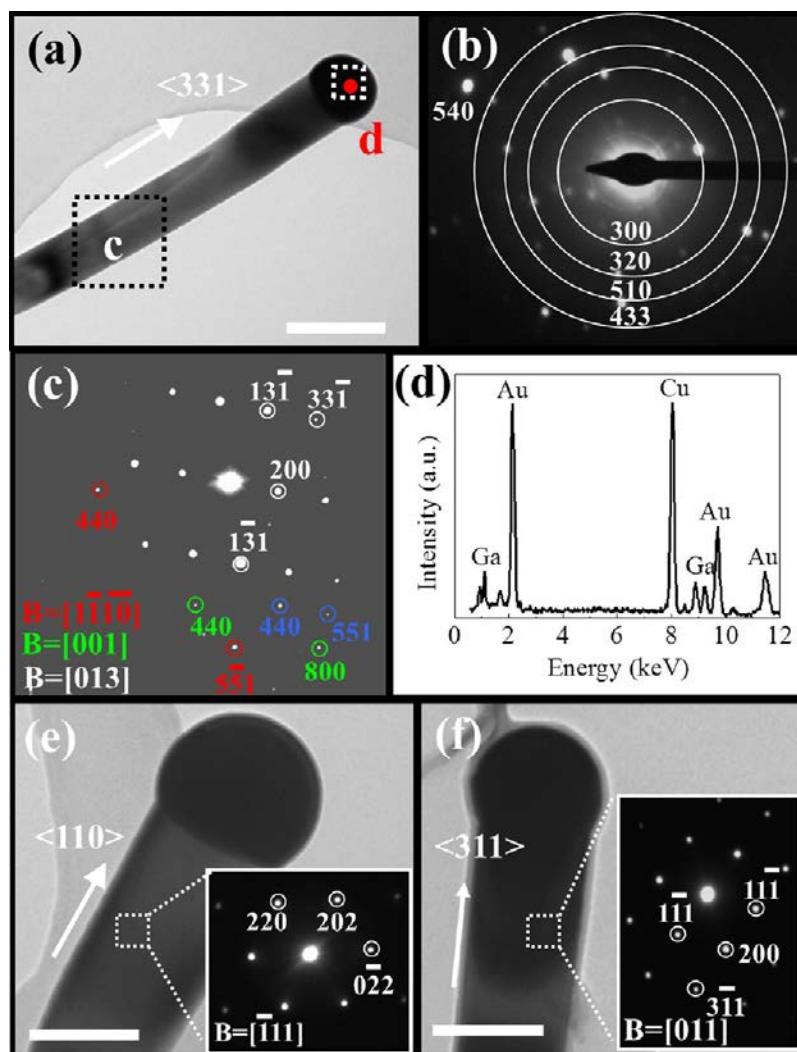
Figure 3. TEM images and SAED patterns of thick NWs grown by multicrystalline Au_7Ga_2 catalysts: (a) one typical NW (d = 120 nm) grown along the $\langle 331 \rangle$ direction (scale bar = 200 nm); (b) SAED pattern of the catalyst tip region b in (a) showing a multicrystalline phase, (c) SAED pattern of the NW body region c in (a) showing a main single crystalline phase indexed in white color, and some crystal defects related patterns indexed in other colors, (d) the EDS spectrum of the catalyst tip spot d in (a), (e) and (f) are typical TEM images and SAED patterns of NWs growing along $\langle 110 \rangle$ and $\langle 311 \rangle$ directions (scale bars = 100 nm).

the growth conditions with the aim to control the crystal phase and orientation of NWs on amorphous substrates, in which various growth orientations such as $\langle 111 \rangle$, $\langle 110 \rangle$, and $\langle 311 \rangle$ GaAs NWs are still being observed due to the lack of crystalline template to direct the NW growth.[14]

At the same time, in addition to aforementioned processing parameters, the growth orientation of NWs are also found to be dependent on the diameter, due to the different stable crystal surfaces at different diameters.[17−19] Theoretical calculation also shows that the surface energy depends not only on the NW diameter and growth temperature, but also on the NW length;[20] therefore, surface energy is not the only factor that determines the NW growth direction. More importantly, since the NW growth initiates at the catalyst/NW interface, the catalytic supersaturation is expected to have a more significant influence over the growth. For example, the trace amount of residual In content or pulsed Ga precursor supply would reduce the Ga supersaturation in Au catalysts, which consequently yield less formation of twin defects in GaP NWs.[21] Also, different composition of Au−In−Ga catalysts would induce different morphologies of InAs NWs grown on GaAs

substrates,[22] while a trace amount of residual In concentration in the Au catalysts resulted from previous growth runs would stabilize the catalysts and alleviate the GaAs NW tapering.[23] However, the effect of catalytic supersaturation on the control of crystal structures, orientation, growth rate and density, etc. during the NW growth is still not well studied and controlled. Recently, we found that GaAs NWs are grown epitaxially from Ni_xGa_y catalyst seeds on amorphous substrates, which determine the crystal phase and growth direction of the NWs accordingly.[24] In this work, here, we further focus on the degree of Ga supersaturation in a more commonly used Au catalyst and present a facile approach to control the crystal structure, defects, orientation, growth rate and density of GaAs NWs via a supersaturation-controlled catalytic engineering process by tailoring the chemical composition and dimension of starting Au_xGa_y catalysts. For the high Ga supersaturation (catalyst diameter <40 nm), NWs can be manipulated to grow unidirectionally along $\langle 111 \rangle$ with the pure ZB phase with a high growth rate, high density and minimal amount of defect concentration utilizing the low-melting-point catalytic alloys (Ga atomic concentration > 30%), whereas for the low Ga
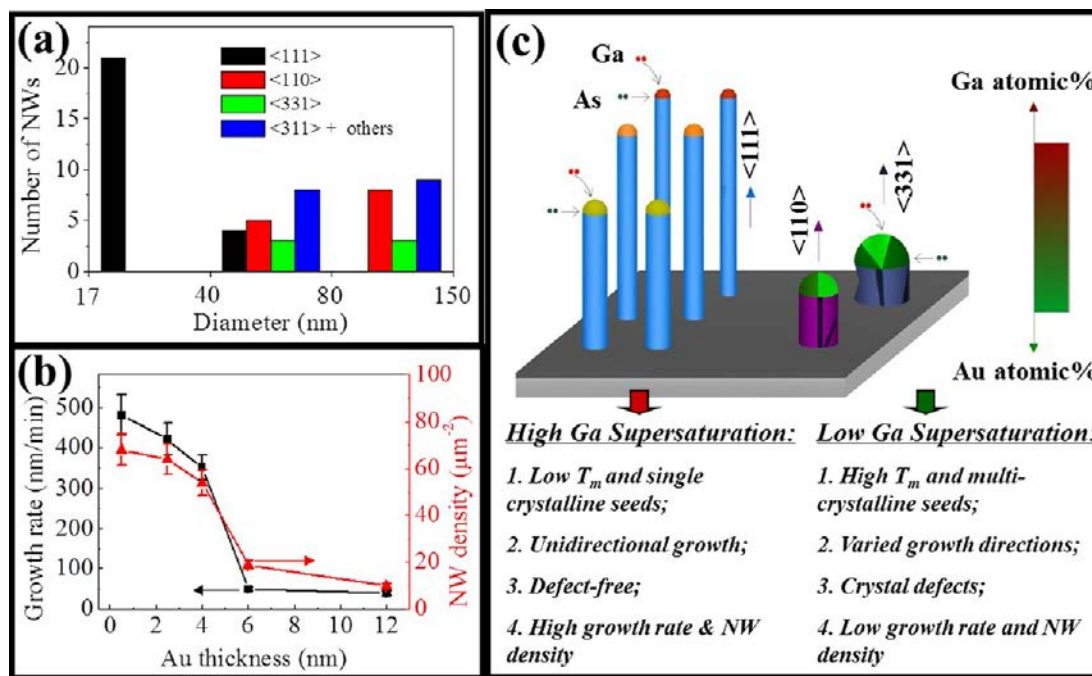
6245

dx.doi.org/10.1021/cg301452d | *Cryst. Growth Des.* 2012, 12, 6243−6249

Figure 4. (a) Growth direction statistics of grown GaAs NWs. The NWs in the diameter range of 17−40 nm are all grown in the ⟨111⟩ direction, while the thick NWs have a mixed orientations of ⟨110⟩, ⟨331⟩, and ⟨311⟩, etc. (b) Change of GaAs NW growth rate and density with different thickness of Au catalyst film (i.e., NW diameter), (c) the schematic illustration of GaAs NW growth rate, density, orientation, and crystal phase change with Ga supersaturation in Au catalyst with different diameters. The higher supersaturation of Ga in small Au particles can provide sufficient Ga precursor by the fast and homogeneous diffusion, thus making the NWs grow faster and in a unidirectional ⟨111⟩ orientation with the highest Ga atomic density.

supersaturation catalytic alloys (catalyst diameter > 40 nm; Ga atomic concentration < 30%), NWs are grown inevitably with a mixed crystal orientation and high concentration of defects.

In this study, GaAs NWs with a diameter range of 17−200 nm are grown by different thicknesses (0.5−12 nm) of Au catalyst films in a chemical vapor deposition (CVD) system,[14,25] as typically shown in scanning electron microscope (SEM) and transmission electron microscope (TEM) images in Figure 1a−c. More importantly, the X-ray diffraction (XRD) patterns depicted in Figure 1d show an overwhelming amount of NWs, with a different starting thickness of Au films, growing in the pure ZB cubic phase (PDF 14-0450) without any detectable WZ phase. It is well-known that the WZ structure is only favored for NWs with a smaller diameter (<10 nm) due to the surface energy change,[26] while the thinnest NWs in our experiments catalyzed by the 0.5 nm thick Au film is still larger than 10 nm; it is therefore consistent that no WZ structure is observed. The pure ZB phase of our grown NWs is also verified by other structural identification of individual NW illustrated in Figures 2 and 3.

In order to study the effect of Ga-rich composition in the catalytic supersaturation, we first focus on the NWs grown with small catalyst diameters (d < 40 nm) since the small Au particles are known to induce a higher degree of Ga supersaturation in the nanoscale.[27] As presented in Figure 2, based on the plane spacings determined in high resolution TEM (HRTEM) and diffraction patterns in fast Fourier transformation (FFT) in the insets, the Au-catalyzed thin NWs (<40 nm) are grown with ZB structure without any significant amount of crystal defects. It is noted that the FFT of NW body in Figure 2b is shown in Supporting Information, Figure S1a as the tip and the body are not observed under the same zone axis. Importantly, all catalytic Au_xGa_y tips are single

crystalline (Figure 2 insets), while the corresponding NWs all grow along the ⟨111⟩ direction. Also, as the NW diameter increases from ∼25 to ∼38 nm (Figure 2a−c), tailored by the increase of catalytic alloy tip diameters, the resultant catalytic Ga concentration decreases accordingly from ∼50 to ∼30 atomic %, equivalent to the stoichiometry of AuGa, Au_2Ga and Au_7Ga_3 alloys as determined by energy dispersive X-ray spectrometric (EDS) spectra as shown in Figure 2d−f. Further decreasing the NW diameter down to ∼17 nm does not increase the Ga composition continuously, as depicted in Figure S1b−d, Supporting Information, but the cubic ZB AuGa phase still exists and preserves. Notably, although the orthorhombic crystal phase and lattice parameters of AuGa and Au_2Ga are consistent with those in the standard card (PDF 29-0619 and 3-065-1488, respectively), the Au_7Ga_3 phase has not been well determined in the literature.[28] By mimicking its Au_7In_3 analogue (hexagonal phase, PDF 29-0647) together with identifying an agreement of the FFT pattern in Figure 2c with one of the hexagonal phase viewing in the $[2\overline{1}\overline{1}0]$ direction, it is determined that the Au_7Ga_3 phase is existed in the hexagonal structure. Simultaneously, after the determination of d-spacings, where $d(0001) = 0.621$ nm, $d(10\overline{1}0) = 0.309$ nm, and $d(10\overline{1}1) = 0.277$ nm from the HRTEM image (Figure 2c), the lattice parameters can be calculated to be $a = b = 0.357$ nm and $c = 0.621$ nm for this hexagonal phase. Furthermore, the thin NWs are typically observed with no crystal phase change or twin defect formation as demonstrated by one representative entire NW in Figure S2, Supporting Information, which grows in the ⟨111⟩ direction in the ZB phase. Also, no post-growth is observed in the cooling step as the Ga and As precursor supply is ceased instantaneously by stopping the heater of the source zone. Therefore, it is unambiguously confirmed that these NWs are free of twins and

other defects. In this case, the high Ga supersaturation (Ga atomic concentration > 30%) tailored by the small starting catalyst dimension (d < 40 nm) has been demonstrated to yield pure ZB phase, unidirectional NWs with a minimal amount of crystal defects in these CVD processes.

Once the diameter of Au catalysts is tuned larger than 40 nm, as illustrated in Figure 3a, the as-obtained thick GaAs NWs typically have polycrystalline alloy tips and NW bodies, indicated by the corresponding selected area electron diffraction (SAED) pattern in Figure 3, panels b and c, respectively. According to the EDS spectrum performed in the tip region (Figure 3d), the thick alloy usually consists of an atomic ratio of Au:Ga ∼ 7:2, suggesting the low Ga composition for the catalytic supersaturation in these thick NWs. Notably, some minor phases may also exist in the tips which cannot be identified by SAED. In addition to the ⟨331⟩ direction (Figure 3a), these thick NWs are also grown with a mixed orientation including ⟨110⟩ in Figure 3e, ⟨311⟩ in Figure 3f and other directions such as ⟨210⟩ and ⟨531⟩ in Supporting Information, Figure S3 as determined by the corresponding SAED patterns in the insets. All of these have indeed revealed the low Ga catalytic composition results in polycrystalline alloy seeds, uncontrollable NW orientations as well as crystal phases for thick NWs.

In order to statistically confirm our experimental observations, more than 60 NWs with different diameters, growth orientations are observed and compiled in Figure 4a. It is clear that all thin NWs in the range of 17−40 nm of diameters are grown in pure ZB phase and along the unidirectional ⟨111⟩ direction, while thick NWs grow with mixed orientations even though in the same cubic ZB structure. It again demonstrates that by just tuning the catalyst particle size (d < 40 nm), the composition of Au$_x$Ga$_y$ alloy tips is manipulated to give single crystalline catalytic phase in the NW growth, which thus leads to a pure ZB phase and unidirectional ⟨111⟩ GaAs NWs without any significant amount of crystal defects. Furthermore, the NW growth rate and density, extracted from the post-growth data (Supporting Information, Figure S4), are also found to decrease with the increase of Au film thickness (i.e., catalyst and NW diameters) as shown in Figure 4b, inferring a fast and efficient Ga diffusion in the homogeneous VLS-like growth mode for higher growth rate in the high Ga supersaturation, which results in the NW formation in lowest free energy {111} GaAs planes along the ⟨111⟩ growth direction. In the low Ga catalytic composition, an insufficient Ga diffusion (or Au-rich detention) exists in the inhomogeneous VSS-like growth mode leading to a slow NW growth rate due to the less and nonuniform Ga precursor precipitation to the growing interface, leading to GaAs NWs stacking in other planes with less dense Ga atoms, and even with crystal defects (Figure 3a).[4] All of these experimental results are summarized in the schematic illustration in Figure 4c.

To further explore the underlying physical principles in the catalytic supersaturation effect on different catalyst dimensions, a simple theoretical simulation is performed to assess the role of Ga supersaturation in Au particles during the NW growth. On the basis of the Gibbs−Thomson effect, it is well-established that Au particles can be supersaturated by Ga in the nanometer scale due to the larger surface energy of nanoparticles, which can be described by the equation of $\ln(C_d/C_0) = 4\gamma V_m/(dRT)$, where C_d is the concentration of Ga in Au nanoparticle with diameter of d, C_0 is the equilibrium concentration in flat surface ($d \rightarrow \infty$) materials, γ is surface

energy (1.39 J m^{-2}), V_m is molar volume of Au (assuming in molten phase, 11.38 cm^3 mol^{-1}), R is constant (8.314 J mol^{-1} K^{-1}), and T is the growth temperature (constant at 873 K for all our growth trials such that Au catalyst particles are only varied with different diameters in this study).[27,29,30] By varying as a function of catalyst diameters, this equation gives a simulated Ga supersaturation curve as shown in Figure 5 (black
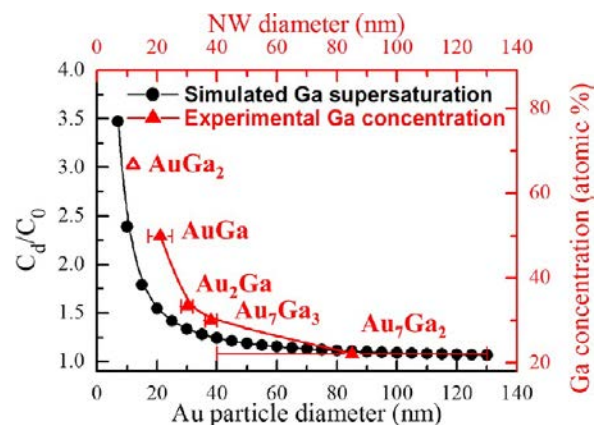

Figure 5. Simulation of the supersaturation of Ga in Au nanoparticles with different diameters (black line) and the experimental results of catalytic Ga concentration with different NW diameters (red line).

colored line with solid circular dots). Comparing our experimental results of 50 (AuGa), 33.3 (Au$_2$Ga), 30 (Au$_7$Ga$_3$), and 22.2 (Au$_7$Ga$_2$) atomic % Ga concentration in different NW diameters (red colored line with solid triangular dots) to the simulated curve, the experimental trend agrees well with the simulation for the exponential increase of Ga supersaturation in the decreasing diameters, assuming a C_0 of 22.2 atomic % Ga concentration. Notably, the small discrepancy between the simulated and experimental results can be attributed to the difference considering simulated spherical Au diameters versus actual hemispherical sizes. A correction of the equivalent Au diameters has been implemented to further fit the results (Supporting Information, Figures S5 and S6).

At the same time, the melting point (T_m) of each corresponding Au$_x$Ga$_y$ alloy composition has been extracted from the binary Au−Ga phase diagram[28] and compiled in Table 1. Surprisingly, all AuGa (T_m = 461.3 °C), Au$_2$Ga (T_m = 339.4 °C) and Au$_7$Ga$_3$ (T_m = 348.8 °C) alloys have the low melting point as compared to the NW growth temperature in this study, while that of Au$_7$Ga$_2$ is relatively higher (T_m ∼ 500 °C). All of these have revealed that in the low Ga catalytic composition (d

Table 1. Properties of Different Au$_x$Ga$_y$ Alloys Extracted from the Binary Au−Ga Phase Diagram[28] and Comparison to Our Experimental Results

catalysts	Ga concentration (atomic %)	melting point (°C)	crystal phase	experimental results
AuGa$_2$	66.7	491.3	cubic	not observed
AuGa	50	461.3	orthorhombic	orthorhombic
Au$_2$Ga	33.3	339.4	orthorhombic	orthorhombic
Au$_7$Ga$_3$	30	348.8	undetermined	hexagonal
Au$_7$Ga$_2$	22.2	∼500	hexagonal	multi crystalline

> 40 nm; Ga atomic concentration <30%), the resultant Au_7Ga_2 alloy probably exists in the solid or solid/liquid phase (not pure catalytic liquid phase) as compared with the Ga-rich cases (d > 40 nm; Ga atomic concentration >30%), and thus a VSS-like growth mechanism is believed to take place for these thick NWs, leading to NWs with different growth orientations and crystal defects induced by inhomogeneous Ga diffusion to the growth front within the polycrystalline catalyst. In the extreme case, even a pure solid phase can exist when the Ga concentration is as low as ~10 atomic %, as verified by electron diffraction in the literature.[4,6] It is also noted that there exists an $AuGa_2$ phase in the phase diagram, which has a much higher Ga concentration of 66.7 atomic %. This super Ga-rich phase is expected to present an even smaller diameter, as indexed in the open triangular dot in Figure 5; however, it also possesses a high melting point of 491.3 °C, similar to that of Au_7Ga_2. As Ga supersaturates Au particles gradually from the low to high concentration, the low-melting-point alloys with low Ga concentrations will precipitate NWs more efficiently and predominantly as compared to the high-melting-point $AuGa_2$ alloy; as a result, no NW grown by the $AuGa_2$ alloy is observed in our experiments.

In summary, an approach to manipulate the Ga super-saturation in Au_xGa_y catalytic alloys, utilizing the manipulation of catalyst dimension and chemical composition, to achieve the pure ZB phase and unidirectional GaAs NWs without any significant amount of crystal defects is presented. Specifically, unidirectional ⟨111⟩ NWs in the diameters of 17−40 nm are presumed to grow via a VLS mechanism with the low-melting-point catalytic alloys of AuGa, Au_2Ga and Au_7Ga_3 in the high Ga supersaturation composition, while thicker NWs are grown via a VSS-like growth mechanism because of the corresponding high melting point Au_7Ga_2 alloy in the low Ga supersaturation regime. In this regard, the composition of catalytic alloys is tunable by tailoring the starting Au film thickness, in a good agreement with the theoretical supersaturation simulation, which demonstrates a versatile approach to control the crystal quality and orientation for the uniform NW growth.

EXPERIMENTAL DETAILS

GaAs NW Synthesis. GaAs NWs used in this study were prepared in a dual-zone horizontal tube furnace as reported in refs 14 and 25. Briefly, the solid source (1 g, GaAs powder, 99.9999% purity, placed in a boron nitride crucible) was evaporated at the center of the upstream zone, while the growth substrate (various thickness of Au film deposited on SiO_2/Si) was placed in the middle of the downstream zone with a tilt angle of ~20° and a distance of 10 cm away from the source. In order to tailor the diameter of Au particles for different catalytic composition and degree of supersaturations, Au films with a thickness of 0.5−12.0 nm were thermally evaporated under a vacuum of ~1×10^{-6} Torr onto the substrates. During the NW growth, the substrate was thermally annealed at 800 °C for 10 min in a hydrogen environment (99.999% pure H_2, 200 sccm, 1 Torr) to obtain Au nanoclusters with different sizes as the catalysts. When the substrate temperature was cooled to the preset growth temperature (590−610 °C), the source was heated to the required source temperature (900−925 °C) for a duration of 0.5−1 h. After the growth, the source and substrate heater were stopped together and cooled down to the room temperature under the flow of H_2 gas.

GaAs NW Characterization. Surface morphologies of the grown NWs were observed with SEM (FEI/Philips XL30) and TEM (Philips CM-20). Crystal structures were determined by collecting XRD patterns on a Philips powder diffractometer using Cu Kα radiation (λ = 1.5406 Å), imaging with a high resolution TEM (JEOL 2100F) and studying with the SAED (Philips CM-20). Elemental mappings were performed using an EDS detector attached to the CM-20 and JEOL 2100F to measure the chemical composition of grown NWs. For the elemental mapping and TEM, GaAs NWs were first suspended in the ethanol solution by ultrasonication and drop-casted onto the grid for the corresponding characterization.

ASSOCIATED CONTENT

⑤ Supporting Information
TEM image of one typical thin and entire NW; cubic phase and growth orientation determination; growth rate and NW density measurement; correction of the experimental results in the Ga supersaturation simulation. This material is available free of charge via the Internet at http://pubs.acs.org.

AUTHOR INFORMATION

Corresponding Author
*E-mail: johnnyho@cityu.edu.hk.
Author Contributions
⊥These authors contributed equally.
Notes
The authors declare no competing financial interest.

ACKNOWLEDGMENTS

REFERENCES

(1) Gudiksen, M. S.; Lauhon, L. J.; Wang, J.; Smith, D. C.; Lieber, C. M. *Nature* **2002**, *415*, 617−620.
(2) Hou, J. J.; Han, N.; Wang, F.; Xiu, F.; Yip, S.; Hui, A. T.; Hung, T.; Ho, J. C. *ACS Nano* **2012**, *6*, 3624−3630.
(3) del Alamo, J. A. *Nature* **2011**, *479*, 317−323.
(4) Persson, A. I.; Larsson, M. W.; Stenstrom, S.; Ohlsson, B. J.; Samuelson, L.; Wallenberg, L. R. *Nat. Mater.* **2004**, *3*, 677−681.
(5) Ihn, S. G.; Song, J. I; Kim, T. W.; Leem, D. S.; Lee, T.; Lee, S. G.; Koh, E. K.; Song, K. *Nano Lett.* **2007**, *7*, 39−44.
(6) Dick, K. A.; Deppert, K.; Karlsson, L. S.; Wallenberg, L. R.; Samuelson, L.; Seifert, W. *Adv. Funct. Mater.* **2005**, *15*, 1603−1610.
(7) Dick, K. A.; Caroff, P.; Bolinsson, J.; Messing, M. E.; Johansson, J.; Deppert, K.; Wallenberg, L. R.; Samuelson, L. *Semicond. Sci. Technol.* **2010**, *25*, 024009.
(8) Thelander, C.; Caroff, P.; Plissard, S.; Dey, A. W.; Dick, K. A. *Nano Lett.* **2011**, *11*, 2424−2429.
(9) Caroff, P.; Dick, K.; Johansson, J.; Messing, M.; Deppert, K.; Samuelson, L. *Nat. Nanotechnol.* **2008**, *4*, 50−55.
(10) Hoang, T. B.; Moses, A. F.; Zhou, H. L.; Dheeraj, D. L.; Fimland, B. O.; Weman, H. *Appl. Phys. Lett.* **2009**, *94*, 133105.
(11) Joyce, H. J.; Wong-Leung, J.; Gao, Q.; Tan, H. H.; Jagadish, C. *Nano Lett.* **2010**, *10*, 908−915.
(12) Joyce, H. J.; Gao, Q.; Tan, H. H.; Jagadish, C.; Kim, Y.; Fickenscher, M. A.; Perera, S.; Hoang, T. B.; Smith, L. M.; Jackson, H. E.; Yarrison-Rice, J. M.; Zhang, X.; Zou, J. *Adv. Funct. Mater.* **2008**, *18*, 3794−3800.
(13) Dhaka, V.; Haggren, T.; Jussila, H.; Jiang, H.; Kauppinen, E.; Huhtio, T.; Sopanen, M.; Lipsanen, H. *Nano Lett.* **2012**, *12*, 1912−1918.
(14) Han, N.; Wang, F. Y.; Hui, A. T.; Hou, J. J.; Shan, G. C.; Xiu, F.; Hung, T. F.; Ho, J. C. *Nanotechnology* **2011**, *22*, 285607.
(15) Fan, Z. Y.; Ho, J. C.; Takahashi, T.; Yerushalmi, R.; Takei, K.; Ford, A. C.; Chueh, Y. L.; Javey, A. *Adv. Mater.* **2009**, *21*, 3730−3743.
(16) Ford, A. C.; Ho, J. C.; Fan, Z. Y.; Ergen, O.; Altoe, V.; Aloni, S.; Razavi, H.; Javey, A. *Nano Res.* **2008**, *1*, 32−39.
(17) Wu, Y.; Cui, Y.; Huynh, L.; Barrelet, C. J.; Bell, D. C.; Lieber, C. M. *Nano Lett.* **2004**, *4*, 433−436.
(18) Wang, C.; Hirano, M.; Hosono, H. *Nano Lett.* **2006**, *6*, 1552−1555.

(19) Cai, Y.; Chan, S. K.; Soar, I. K.; Chan, Y. T.; Su, D. S.; Wang, N. *Adv. Mater.* **2006**, *18*, 109−114.

(20) Cai, Y.; Chan, S. K.; Sou, I. K.; Chan, Y. F.; Su, D. S.; Wang, N. *Small* **2007**, *3*, 111−115.

(21) Johansson, J.; Karlsson, L. S.; Dick, A. C.; ZBolinsson, J.; Wacaser, B. A.; Deppert, K.; Samuelson, L. *Cryst. Growth Des.* **2009**, *9*, 766−773.

(22) Bauer, J.; Gottschalch, V.; Wagner, G. *J. Appl. Phys.* **2008**, *104*, 114315.

(23) Dick, K. A.; Deppert, K.; Samuelson, L.; Wallenberg, L. R.; Ross, F. M. *Nano Lett.* **2008**, *8*, 4087−4091.

(24) Han, N.; Hui, A. T.; Wang, F.; Hou, J. J.; Xiu, F.; Hung, T. F.; Ho, J. C. *Appl. Phys. Lett.* **2011**, *99*, 083114.

(25) Han, N.; Wang, F.; Hou, J. J.; Xiu, F.; Yip, S.; Hui, A. T.; Hung, T.; Ho, J. C. *ACS Nano* **2012**, *6*, 4428−4433.

(26) Shtrikman, H.; Popovitz-Biro, R.; Kretinin, A.; Houben, L.; Heiblum, M.; Bukała, M.; Galicka, M.; Buczko, R.; Kacman, P. *Nano Lett.* **2009**, *9*, 1506−1510.

(27) Zhang, G. Q.; Tateno, K.; Sanada, H.; Tawara, T.; Gotoh, H.; Nakano, H. *Appl. Phys. Lett.* **2009**, *95*, 123104.

(28) Massalski, T.; Okamoto, H.; Subramanian, P.; Kacprzak, L. *Binary Alloy Phase Diagrams*; ASM International, Materials Park, Ohio, USA, 1990; Vol. 3.

(29) Lide, D. R. *CRC Handbook of Chemistry and Physics*; CRC Press: Boca Raton, 2010.

(30) Porter, D. A.; Easterling, K. E. *Phase Transformations in Metals and Alloys*; London: Chapman & Hall, 1992.